

Controls of land surface and bedrock topography on the spatial distributions of water table and storage: unifying saturation excess runoff models

Lili Yao¹ and Dingbao Wang¹

¹University of Central Florida

November 23, 2022

Abstract

The control of land surface topography on the configuration of groundwater table has been recognized and well explored. However, the control of bedrock topography on water table is much less studied, potentially due to the limited observations of bedrock. This paper evaluates the controls of both surface and subsurface topography on the spatial distributions of steady-state water table and the corresponding water storage at the catchment scale based on numerical simulations. Numerical models with different topographic features are developed using MODFLOW (USG). When water table is shallow, the control on the spatial distributions of water table is dominated by land surface topography (i.e., water table is approximately parallel to land surface); with the increase of water table depth, the role of land surface topography decreases; when water table is deep and close to bedrock surface, the spatial distributions of water table is dominated by bedrock topography (i.e., water table is approximately parallel to bedrock surface). For land surface-dominated water table, storage capacity in unsaturated area is spatially uniform, which is the underlying assumption of TOPMODEL; however, for bedrock-dominated water table, water storage in unsaturated area is spatially uniform, which is the underlying assumption of VIC-type model. The systematical variations of the controls of surface and subsurface topography on water table configuration provide a framework to unify saturation excess runoff models by treating TOPMODEL and VIC-type model as two endmembers.

1 **Controls of land surface and bedrock topography on the spatial distributions of water table**
2 **and storage: unifying saturation excess runoff models**

3 Lili Yao and Dingbao Wang*

4 Department of Civil, Environmental, and Construction Engineering, University of Central Florida, Orlando,
5 Florida, USA

6 *Correspondence to: dingbao.wang@ucf.edu
7

8 **Abstract**

9 The control of land surface topography on the configuration of groundwater table has been
10 recognized and well explored. However, the control of bedrock topography on water table is much
11 less studied, potentially due to the limited observations of bedrock. This paper evaluates the
12 controls of both surface and subsurface topography on the spatial distributions of steady-state
13 water table and the corresponding water storage at the catchment scale based on numerical
14 simulations. Numerical models with different topographic features are developed using
15 MODFLOW (USG). When water table is shallow, the control on the spatial distributions of water
16 table is dominated by land surface topography (i.e., water table is approximately parallel to land
17 surface); with the increase of water table depth, the role of land surface topography decreases;
18 when water table is deep and close to bedrock surface, the spatial distributions of water table is
19 dominated by bedrock topography (i.e., water table is approximately parallel to bedrock surface).
20 For land surface-dominated water table, storage capacity in unsaturated area is spatially uniform,
21 which is the underlying assumption of TOPMODEL; however, for bedrock-dominated water table,
22 water storage in unsaturated area is spatially uniform, which is the underlying assumption of VIC-
23 type model. The systematical variations of the controls of surface and subsurface topography on
24 water table configuration provide a framework to unify saturation excess runoff models by treating
25 TOPMODEL and VIC-type model as two endmembers.

26 **Keywords:** Water table; Topography; Bedrock; TOPMODEL; VIC; Saturation excess

27

28 **Key points:**

29 1. The configuration of groundwater table emulates the subsurface (surface) topography at deep
30 (shallow) water table.

31 2. For land surface-dominated water table, storage capacity in unsaturated area is spatially uniform
32 (TOPMODEL).

33 3. For bedrock-dominated water table, water storage in unsaturated area is spatially uniform (VIC-
34 type model).

35

36 **1. Introduction**

37 Groundwater table is an important hydrologic interface controlling water exchange
38 between surface and subsurface (Condon, et al., 2020; Ferguson & Maxwell, 2010; Hooshyar &
39 Wang, 2016; Liang et al., 2003; Maxwell & Condon, 2016; Spence et al., 2009). The depth of
40 water table at the catchment scale varies spatially (Condon & Maxwell, 2015), and the
41 configuration of water table is directly related to the spatial distribution of water storage which
42 determines the locations of source area for runoff generation and how much rainfall could be
43 retained underground during a saturation excess runoff process (Appels et al., 2017; Berghuijs et
44 al., 2016; Kollet & Maxwell, 2008; Soyly et al., 2011).

45 The configuration of water table has been widely simplified as the subdued replica of
46 topography (Cardenas, 2007; Jiang et al., 2010; Micallef et al., 2020; Toth, 1963; Zhang et al.,
47 2020). Though studies have confirmed the benefit from this simple conceptualization, it has been
48 found that water table is not always highly correlated to the land surface topography (Condon &

49 Maxwell, 2015; Desbarats et al., 2002; Grayson & Western, 2001; Shaman et al., 2002). To
50 quantify the extent of water table interactions with land surface topography, a dimensionless
51 number called water table ratio, which is defined as the ratio of potential groundwater mounding
52 to topographic relief, was proposed by Haitjema & Mitchell-Bruker (2005). They categorized
53 water table into two types: topography-controlled or recharge-controlled. Topography-controlled
54 water table is closely connected to land surface topography and is more likely developed in humid,
55 low-permeability terrain; whereas, recharge-controlled water table is more disconnected from the
56 land surface topography and more likely occurs in arid, more permeable terrain (Haitjema &
57 Mitchell-Bruker, 2005). The topography-controlled water table is often associated with shallow
58 water table depth, whilst the recharge-controlled water table commonly has a deep water table
59 depth (Cuthbert et al., 2019; Gleeson & Manning, 2008). It is worth noting that this categorization
60 does not account for the effect of subsurface topography since they assumed a deep horizontal
61 bedrock.

62 Groundwater in unconfined aquifer is vertically constrained by both the land surface and
63 the hydrological impeding layer. The latter could be a fresh bedrock or a soil layer with hydraulic
64 conductivity several orders of magnitude lower than that of the surficial soil formation (Condon,
65 et al., 2020; Freeze & Cherry, 1979). For the sake of brevity, we will refer to the hydrological
66 impeding layer that restricts percolation as bedrock in this paper. The use of geophysical
67 techniques revealed that the underlain bedrock topography can be substantially different from the
68 land surface topography (McDonnell et al., 1996; St. Clair et al., 2015; Zimmer & McGlynn,
69 2017). Considering that the bedrock is the lower boundary of groundwater, one may be curious
70 about the role of bedrock topography on the configuration of groundwater table. However, the
71 correlation between bedrock and groundwater table is much less studied because it is not easy to

72 obtain the details of bedrock topography at large spatial scales. Whilst, a number of studies
73 focused on hillslope-scale processes have identified that bedrock topography was one of the most
74 important physical characteristics affecting the response of groundwater to rainfall (Bachmair &
75 Weiler, 2012; Freer et al., 2002). The topography of bedrock surface was found to exert a key
76 control on the hydrological connectivity of subsurface drainage network (Penna et al., 2015;
77 Tromp-van Meerveld & McDonnell, 2006).

78 Since both land surface and bedrock topography are important controls on the groundwater,
79 the question then is under what circumstances does the land surface topography dominantly control
80 the water table and under what circumstances does bedrock dominantly control the water table.
81 Based on observations at the hillslope scale, van Meerveld et al. (2015) and Hutchinson & Moore
82 (2000) reported that the shapes of water table change with groundwater levels, and water table
83 configuration follows land surface topography when the water table is shallow, whereas, water
84 table configuration follows bedrock topography when the water table is close to the bedrock.
85 However, much uncertain still exists about the control of land surface and bedrock surface
86 topography on the groundwater configuration and the corresponding water storage distribution at
87 the catchment scale due to the limitation of bedrock information as mentioned previously.

88 Characterizing the antecedence wetness condition in the catchment is a prerequisite for the
89 saturation excess runoff modeling. As the two most popular saturation excess runoff models, the
90 TOPMODEL and the Probability Distributed Model (PDM) adopt different methods for the
91 conceptualization of antecedence wetness condition. In the TOPMODEL, the hydraulic gradient
92 of groundwater is assumed to be same as the gradient of land surface topography, and the position
93 of water table is treated to rise or fall with spatially uniform amounts (Beven & Kirkby, 1979;
94 Sivapalan et al., 1987). Tough it is known that water table does not always mirror land surface, it

95 is still a reasonable simplification in regions with topography-controlled water table (Rinderer et
96 al., 2014; Troch et al., 1993). The PDM includes the Xinanjiang model (Zhao, 1992), VIC model
97 (Liang et al.,1994), and HyMOD (Moore, 1985), and we will use the VIC-type model to refer to
98 the PDM hereinafter. Different from TOPMODEL, VIC-type model explicitly characterizes water
99 storage instead of the position of water table. To facilitate the development of water balance
100 equations, the spatial variability of maximum water storage capacity in VIC-type model is
101 quantified using a cumulative distribution function, such as the generalized Pareto distribution
102 function (Liang et al., 1994; Zhao, 1992) and the SCS distribution function (Yao et al., 2020).
103 However, to the best of our knowledge, the underlying water table configuration inferred from the
104 storage distribution of the VIC-type model is not discussed in the literature yet.

105 Both the TOPMODEL and VIC-type model have a hypothesis on the configuration of
106 groundwater table. This leads to the question that if there is any linkage between these two models.
107 As mentioned, the critical assumption about the water table configuration in TOPMODEL is more
108 valid in regions where the water table is close to the land surface topography (i.e., shallow water
109 table). However, it is unknown about the connection between the topography and the water table
110 assumed in VIC-type model, and neither the suitability of VIC-type model at different water table
111 conditions considering its underlying assumption on the water table configuration.

112 The objective of this paper is to gain a better understanding of the spatial pattern of
113 groundwater table and water storage at the catchment scale with considerations of surface and
114 subsurface topography. It will also shed light on the saturation excess runoff models regarding
115 their assumptions of the groundwater table configuration. To achieve these goals and considering
116 the limitation of the available observation data in the reality, we conduct numerical simulations to
117 model groundwater flow under different conditions. The second section introduces the

118 topographic information of the model domain, and the main features of the numerical model.
119 Section 3 presents the spatial distributions of water table and storage at different bedrock settings,
120 and discusses the implication of the findings to the unification of saturation excess runoff models.
121 The final section summaries the main findings of this paper.

122

123 **2. Methodology**

124 The purpose of this paper is not to develop a numerical model for the groundwater system
125 in a specific catchment, but to gain understanding about the controls of catchment properties on
126 the spatial distributions of water table and storage at different steady-state groundwater levels.
127 Therefore, a series of hypothetical models are developed in this paper.

128 **2.1 Land surface topography**

129 The numerical model domain is bounded by the land surface topography on the top, and
130 the selected model area is the Crab Orchard Creek catchment located in Illinois (USGS gauge ID:
131 05597500) with a drainage area of approximately 80 km². The land surface elevation in the
132 catchment ranges from 129 to 185 m above mean sea level as presented in Figure 1a. The average
133 land surface slope is 0.017. The stream network on the land surface shown in Figure 1a was
134 extracted from the digital elevation model (DEM) with a resolution of 30 m, and the “slope-
135 drainage area” relation was used to determine the origin of the stream network (Tromp &
136 McDonnell, 2006), which is approximately 0.14 km² for the model area. The highest stream order
137 in the study catchment is 5.

138 **2.2 Bedrock topography**

139 Investigating the role of bedrock topography on the water table configuration is one of the
140 main objectives in this paper. The observed bedrock of the model domain is shown in Figure 1b

141 (Data source is provided in the Acknowledgement section), and the average soil thickness (AST),
142 i.e., the vertical distance between land surface and bedrock surface, is 10 m. Bedrock topography
143 may be similar with land surface topography such as that in the model area, while the similarity of
144 topographies between land surface and bedrock surface may vary among catchments (Freer et al.,
145 1997). To explore the effect of bedrock topography on water table configurations, a series of
146 synthetic bedrocks are generated in this paper. Though bedrock surface at the hillslope scale has
147 been simplified as geometric abstractions using mathematical functions such as second-order
148 polynomial function and curvature function (Fan & Bras, 1998; Troch et al., 2002), there is no
149 uniform method to conceptualize the bedrock surface at the catchment scale. To facilitate practice,
150 we proposed to utilize the observed bedrock data combined with stream network on the land
151 surface to generate synthetic bedrocks.

152 The elevation (E [m]) of a synthetic bedrock at the point scale is generated by the following
153 equation:

$$154 \quad E = E_0 + s \times d \quad (1)$$

155 where E_0 [m] is the observed bedrock elevation of the closest cell in the stream network; s [-] is
156 the slope of the bedrock between the cell and its closest cell, and is set to 0.002 in this study; d
157 [m] is the horizontal component of the minimum downslope distance to a cell on the stream
158 network, following the flow path. Since the slope of land surface is higher than 0.002, the soil
159 depth for the generated bedrocks increases from channel to upland, which has been widely
160 observed in nature and used in conceptual models (Rempe & Dietrich, 2014; St. Clair et al., 2015;
161 Troch et al., 2002; Zimmer & McGlynn, 2017). The stream network used for determining the
162 values of E_0 and d includes different orders of streams when generating different bedrocks. The
163 bedrock, which is generated using the completed stream network, is called as the 1st-order bedrock

164 and shown in Figure 2a. While, the 1st-order streams are excluded from the stream network when
165 generating the 2nd bedrock which is called as the 2nd-order bedrock and shown in Figure 2b.
166 Likewise, the 2nd-order, 3rd-order, and 4th-order streams are excluded from stream network when
167 generating the 3rd, 4th, and 5th-order bedrock, respectively. Therefore, the topography of bedrock
168 surface inherits less and less topographic information of land surface from the 1st to the 5th-order
169 bedrock (Figures 2a~e). Among the 5 synthetic bedrocks, the 2nd-order bedrock (Figure 2b) has
170 the highest similarity with the observed bedrock (Figure 1b), and their average difference of the
171 cell-scale elevation is -0.05 m with a range from -12 m to 14 m. Noted that Figures 2a~e show the
172 elevation relative to the lowest point in each synthetic bedrock.

173 To explore the control of bedrock surface topography on the water table configuration,
174 numerical models #1-#5 with the 1st-order to 5th-order bedrocks are developed, and they are
175 controlled to have the same AST (10 m, as same as the observation) by raising or falling the
176 bedrock surface with a spatially uniform amount. In addition, to investigate the role of soil
177 thickness on the water table, model #6 with the 2nd-order bedrock but with a different AST (i.e.,
178 13 m) is further developed for comparison with model #2.

179 **2.3 Spatial distribution of water table**

180 The spatial distribution of the steady-state water table is obtained via numerical simulation
181 using MODFLOW (USG) (Panday et al., 2013). The modeled domain is horizontally discretized
182 into finite difference square cells with a resolution of 100 m × 100 m, leading to a total number of
183 8019 cells. The model is not discretized vertically considering that the soil thickness is much
184 smaller than the horizontal dimensions by two to five orders of magnitude. A “drain” boundary
185 condition is assigned to the top face of each grid (Goderniaux et al., 2013). Drain boundary is a
186 head-dependent flux boundary, through which water leaves groundwater system when the head is

187 higher than the land surface elevation, and it turns inactive when the head of the model cell drops
 188 below the land surface (McDonald & Harbaugh, 1998). Discharge of groundwater from an active
 189 drain surface is proportional to the drain conductance, which is assumed to be $10^6 \text{ m}^2/\text{year}$ in this
 190 paper and is subject to change as needed. A spatially uniform recharge is applied to the model
 191 domain, and different steady-state groundwater levels are obtained by adjusting the value of
 192 recharge. The recharge considered here is the net recharge since evaporation is not considered
 193 directly in this paper. All other lateral and vertical edges of the model are set as no-flow
 194 boundaries. The saturated hydraulic conductivity is assumed to be homogeneous and isotropic.
 195 Given land surface and bedrock topography, the ratio of recharge and saturated hydraulic
 196 conductivity determines water table configuration, therefore, the absolute value of the saturated
 197 hydraulic conductivity (i.e., 315 m/year in this paper) is less important here (Gleeson & Manning,
 198 2008; Haitjema & Mitchell-Bruker, 2005).

199 **2.4 Soil water storage**

200 Soil water storage in a soil column referred in this paper includes both the groundwater in
 201 the saturated zone and the soil moisture in the unsaturated zone. The groundwater storage in the
 202 saturated zone is calculated as the groundwater thickness multiplied by the soil porosity. It is
 203 assumed that the vertical distribution of soil moisture is at hydraulic equilibrium condition in the
 204 unsaturated zone (e.g., Yao et al., 2018), and the Brooks-Corey model is used for estimating the
 205 soil moisture distribution (Brooks & Corey, 1964):

$$206 \quad \theta(z) = \begin{cases} (\theta_s - \theta_r) \left(\frac{L-z}{|\varphi_a|}\right)^{-\lambda} + \theta_r, & Z \leq L - |\varphi_a| \\ \theta_s, & , Z > L - |\varphi_a| \end{cases} \quad (2)$$

207 where θ [-] is volumetric soil water content; z [m] is the depth measured from soil surface
 208 (positive downward); θ_r [-] and θ_s [-] are the residual and saturated water content, respectively;

209 φ_a [m] is the bubbling pressure; λ [-] is the pore-size distribution index; and L [m] is the distance
 210 between land surface and groundwater table. The total water storage (S [m]), including the water
 211 below and above the groundwater table in each cell is calculated as follows:

$$212 \quad S = \begin{cases} \int_0^{L-|\varphi_a|} \theta(z) dz + (D + |\varphi_a|)\theta_s, & L > |\varphi_a| \\ (L + D)\theta_s, & L \leq |\varphi_a| \end{cases} \quad (3)$$

213 where D [m] is the groundwater thickness above the bottom of the grid cell. Substituting Equation
 214 (2) into Equation (3), one obtains:

$$215 \quad S = \begin{cases} \frac{\theta_s - \theta_r}{(\lambda - 1)|\varphi_a|^{-\lambda}} (|\varphi_a|^{-\lambda+1} - L^{-\lambda+1}) + (L - |\varphi_a|)\theta_r + (D + |\varphi_a|)\theta_s, & L > |\varphi_a| \\ (L + D)\theta_s, & L \leq |\varphi_a| \end{cases} \quad (4)$$

216 The cell-scale water storage is calculated for each steady-state simulation.

217

218 **3. Results and discussions**

219 **3.1 Spatial distribution of maximum storage capacity**

220 The maximum storage capacity is defined as the total soil water storage space from land
 221 surface to bedrock surface. For homogeneous soil, the spatial variability of maximum storage
 222 capacity is dependent on the spatial variability of soil thickness which is determined by land
 223 surface and bedrock topography. The impact of bedrock topography on the spatial distribution of
 224 maximum storage capacity is obtained by comparing the models with each of the 5 synthetic
 225 bedrocks (Figure 2), i.e., model #1-#5. Figure 3a shows the empirical cumulative distribution
 226 function (CDF) of the normalized maximum storage capacity, i.e., the cell-scale storage capacity
 227 is normalized by its average value over the catchment (the product of 10 m and soil porosity). It
 228 can be found that each CDF presents an “S” shape, which is accordance with previous studies (Gao
 229 et al., 2020; Sivapalan et al., 1997). It is also found that the distributions of the maximum storage

230 with the 1st and 2nd-order bedrocks are very close to the observation. The distributions with the
231 3rd, 4th, and 5th-order bedrocks are similar, and have a larger fraction of the catchment area with
232 high storage capacity.

233 The SCS distribution (Wang, 2018) is used to model the spatial distribution of the
234 maximum storage capacity:

$$235 \quad F(x) = 1 - \frac{1}{a} + \frac{x+(1-a)}{a\sqrt{(x+1)^2-2ax}} \quad (5)$$

236 where x [-] is the normalized maximum storage capacity at cell scale; $F(x)$ is the fraction of the
237 catchment area for which the normalized maximum storage capacity is less than or equal to x ; a
238 [-] is the shape parameter describing the spatial variability of the maximum storage capacity with
239 a range from 0 to 2, and a smaller value of a indicates a larger catchment area with low storage
240 capacity. The shape parameter of each model is obtained by fitting the normalized value of the
241 maximum storage against Equation (5) using the non-linear least square method.

242 The small difference of the distribution in Figure 3a suggests that the shape of bedrock
243 does not significantly influence the spatial distribution of the maximum storage capacity, and this
244 is attributed to the large soil thickness considered in this paper. Compared with the shape of
245 bedrock, soil thickness has a larger impact on the spatial variability of the maximum storage
246 capacity. Figure 3b presents the empirical CDFs of the normalized maximum storage capacity for
247 the model domain with the shape of the 2nd-order bedrock but having different average soil
248 thicknesses by moving the bedrock downward with a spatially uniform value. Figure 3b shows
249 that as soil thickness increases, the lower portion of the CDF moves upward while the upper
250 portion moves downward, leading to a larger shape parameter. It suggests that the spatial
251 variability of the maximum storage capacity decreases as the mean thickness increases, and it is

252 because that the increasing thickness offsets the dispersion of maximum storage capacity at the
253 cell scale.

254 Results show that the shape parameter increases systematically as the AST increases which
255 has significant impacts on the saturation excess runoff production. Gao et al. (2020) found that
256 the runoff generation is sensitive to shape parameter, especially when the shape parameter is close
257 to its upper limit (i.e., 2). Specifically, the saturation excess runoff decreases as the shape
258 parameter increases because a larger shape parameter indicates a larger percentage of catchment
259 area having large maximum storage capacity, therefore more precipitation is retained by the soil
260 for evaporation between precipitation events. Based on the principle of VIC-type model (Liang et
261 al., 1994; Moore, 2007), the amount of soil wetting during a precipitation event (P) is the
262 integration below the CDF curve along y-axis from the initial storage state (C) to the storage state
263 with the amount of precipitation ($C + P$) (see Figure 10a). Correspondingly, runoff is the
264 difference between the precipitation depth and the soil wetting. Therefore, for given mean
265 maximum storage capacity and precipitation depth, if the catchment is under a dry condition which
266 means the antecedent storage occupies only a small portion of the distribution, the catchment with
267 a smaller shape parameter favorites the runoff generation; whereas, if the catchment is wet when
268 the antecedent storage extends to the upper part of the distribution, the catchment with a larger
269 shape parameter create favorable conditions for runoff generation.

270 **3.2 Water table configuration**

271 As mentioned in Section 2.3, mean water table depth in each model is directly determined
272 by the ratio of recharge and saturated hydraulic conductivity (R/K); therefore, a series of water
273 tables with mean depths from 0.5 m to 8 m were obtained by adjusting the values of R/K during
274 simulations for each model, e.g., R/K ranges from 0.002 to 6.3E-08 for the model with the 1st-

275 order bedrock (AST=10 m). As mentioned in the Introduction section, groundwater is bounded
276 by the land surface on the top and the bedrock surface on the bottom; therefore, groundwater table
277 configuration is supposed to be controlled by the topography of both land surface and bedrock
278 surface. Figure 4 displays the groundwater tables for the 5 synthetic bedrocks (AST=10 m) at 3
279 recharge conditions: WTD = 1.5 m, WTD = 4 m, and WTD = 8 m. For given land surface and
280 bedrock surface, the similarity between water table and land surface topography decreases as the
281 mean water table depth increases. When WTD = 1.5 m, the spatial variability of water table
282 (Figure 4a1-4e1) in each model is almost identical to the land surface topography (Figure 1a),
283 whereas, the water table (Figure 4a2-4e2) is much smoother when the mean water table drops to 4
284 m, and the water table (Figure 4a3-4e3) is much different from the land surface when WTD = 8
285 m. The decreasing similarity between water table and land surface confirms the decreasing control
286 of land surface topography on the shape of water table as the mean water table depth increases
287 (Cuthbert et al., 2019; Gleeson & Manning, 2008).

288 Conversely, the role of bedrock topography is more and more significant in determining
289 water table configuration as the water table declines. By comparing the different configurations
290 of water table for given land surface and bedrock (e.g., the 2nd-order bedrock shown in Figure 2b),
291 it is found that the similarity between water table configuration and bedrock topography increases
292 as the WTD increases (Figures 4b1, 4b2, and 4b3). When water table depth is large (e.g., WTD =
293 8 m), the distribution of water table elevation is highly similar with that of bedrock regardless the
294 topography of bedrock (Figures 4a3-e3), and the water table configuration displays less variations
295 within the model domain from the model with the 1st-order to that with the 5th-order bedrock which
296 is accordance with the bedrock topography.

297 The similarity between water table and bedrock is directly determined by the vertical
 298 distance between water table and bedrock (DWB) instead of the water table depth. The 5 models
 299 in Figure 4 have the same AST (=10 m), therefore, the same water table depth means the same
 300 distance between water table and bedrock. To demonstrate the impact of DWB on water table
 301 configuration, Figure 5 shows the spatial distributions of water table for the 2nd-order bedrock with
 302 AST=13 m. When WTD = 8 m, the average DWB is 2 m when AST=10 m (Figure 4b3) and 5 m
 303 when AST=13 m (Figure 5a). It is obvious that the water table with a smaller DWB is more like
 304 the topography of bedrock (Figure 2b). While, when the DWB decreases to 2 m in the case of
 305 AST=13 m, Figure 5b shows that the shape of water table is also similar to that of bedrock.

306 To quantitatively compare the groundwater table configuration with land surface or
 307 bedrock topography, we compute the vertical separation between water table and land surface or
 308 bedrock at the cell scale following Hutchinson & Moore (2000):

$$309 \quad d_{lw,i} = z_{l,i} - z_{w,i} \quad (6)$$

$$310 \quad d_{wb,i} = z_{w,i} - z_{b,i} \quad (7)$$

311 where, $z_{l,i}$ [m], $z_{b,i}$ [m], and $z_{w,i}$ [m] are the elevations of land surface, bedrock surface, and water
 312 table at grid cell i , respectively; $d_{lw,i}$ [m] and $d_{wb,i}$ [m] are the vertical distances between water
 313 table and land surface, and between water table and bedrock surface at grid cell i , respectively.
 314 The standard deviation of $d_{lw,i}$ and $d_{wb,i}$ represents the difference between the shapes of water
 315 table and surface and subsurface topography, and a larger standard deviation means a larger
 316 difference.

317 Figure 6 shows the standard deviations versus the mean water table depth for the 1st-order
 318 to the 5th-order bedrock with AST=10 m. It can be found that at smaller water table depth, the

319 standard deviation with respect to bedrock is larger than that to land surface, while at larger water
320 table depth, the standard deviation with respect to land surface is larger than that to bedrock.
321 Figure 6 confirms the results from Figures 4 and 5 that water table configuration is more controlled
322 by land surface when the water table is shallow but is more controlled by bedrock when the water
323 table is close to the bedrock. It is noted that in the middle range of water table depths, both standard
324 deviations are quite large, which means neither land surface nor bedrock is a reasonable proxy for
325 the water table configuration. These results are in agreement with the field observations at the
326 hillslope scale (van Meerveld et al., 2015; Hutchinson & Moore, 2000). In addition, Figure 6
327 shows that standard deviation with respect to bedrock is quite different among models with
328 different bedrocks. At large water table depth (e.g., mean water table depth = 8 m), the standard
329 deviation (the most right triangular) decreases from the 1st-order to the 5th-order bedrock. That is
330 because the microtopographic features on the bedrock surface are smoothed from the 1st-order to
331 the 5th-order bedrock, correspondingly, the groundwater thickness is increasingly uniform.

332 **3.3 Spatial distribution of water storage**

333 It is intuitive that the amount of water storage decreases as the groundwater table depth
334 increases. However, how does the spatial distribution of water storage change with mean water
335 table depth has not been investigated yet. Figure 7 presents the empirical CDFs of the water
336 storage at different mean water table depths (WTDs) for simulations with the 1st-order to the 5th-
337 order bedrock and with 10 m of average soil thickness, in which the cell-scale storage includes
338 groundwater storage and unsaturated zone storage calculated by Equation (4) with the hydraulic
339 parameters of the Brook-Corey model for sand as shown in Table 1 (Rawls et al., 1982). The black
340 curves in Figure 7 presents the empirical CDF of the maximum storage capacity. It is clear that
341 the spatial distribution of storage evolves systematically with water table depth. The dynamics of

342 the storage distribution is a result of groundwater flows, including the local, inter-mediate, and
343 regional flows, which redistribute the recharged water after it reaches the water table although the
344 applied recharge is uniform over the land surface, and groundwater flow system changes with
345 mean water table depth (Detty & McGuire, 2010; Toth, 1963).

346 Given a shallow water table depth, the spatial distributions of water storage are close to the
347 distribution of their maximum storage capacity which are similar among models with different
348 bedrocks as shown in Figure 3a. The similar distributions of storage at shallow water table confirm
349 that the spatial distribution is dominated by the land surface topography when the water table is
350 shallow. The spatial distributions of water storage become increasingly different among the
351 models as the water table depth increases, indicating the role of bedrock topography in affecting
352 the spatial distribution of water storage at deep water table depth conditions which is consistent
353 with the results for water table configuration in Figures 4 and 6.

354 Given land surface and bedrock topography, the empirical CDF of water storage gradually
355 deviates from an “S” shape as the mean water table depth increases, and the slope of the middle
356 part of the CDF curve decreases as the mean water table depth increases especially for the 4th and
357 5th-order bedrocks. The flatter CDF curve suggests a larger percentage of the catchment area
358 having similar water storage. For simulations with the 1st, 2nd, and 3rd-order bedrocks, a large
359 number of cells have small amount of water storage in the north, the southeast, and the west when
360 WTD = 8 m because of the relatively steep bedrocks in these regions, and the storage is mainly
361 distributed in the downstream, leading to the abrupt change of the slope of the CDF curve.
362 Whereas, less microtopographic features are developed in the 4th-order and 5th-order bedrock
363 leading to the more spatially uniform water storage when WTD = 8 m.

364 **3.4 Effect of hydraulic properties of soil on the distribution of water storage**

365 Though the hydraulic properties of soil (e.g., residual and saturated moisture content, pore-
366 size distribution index, and bubbling pressure) do not determine the position of water table directly,
367 they play an important role in affecting the soil moisture profile in the unsaturated zone above
368 water table. Therefore, the type of soil affects the amount of water storage and its spatial
369 variability. Figure 8 presents the spatial distribution of water storage for clay (the hydraulic
370 properties are shown in Table 1) with the same groundwater table depths as those in Figure 7. The
371 empirical CDF curve gradually deviates from the distribution of maximum storage capacity
372 gradually as the mean water table depth increases, and this result is consistent with the conclusion
373 for sand in Figure 7. However, it can be found that given land surface and bedrock topography,
374 the difference in the spatial distributions of water storage between different water table depths is
375 smaller for clay than for sand. For example, the difference between the CDF for WTD = 8 m and
376 that for WTD = 0.5 m is much smaller in Figure 8a compared with Figure 7a. That is because the
377 larger capillary effect in clay increases the water holding capability in the unsaturated zone, leading
378 to the smaller difference of water storage between conditions with different water table depths.

379 **3.5 Percentage of saturated land surface**

380 The percentage of saturated area on the land surface is an important factor for determining
381 runoff generation since precipitation falls on the saturated area transfers to surface runoff directly.
382 Saturated area occurs where the groundwater table intercepts with land surface; therefore, the
383 percentage of saturated area changes with water table depth. Figure 9 presents the percentage of
384 saturated area (defined as the ratio between the flooded area and the total area in the model) as a
385 function of mean water table depth for simulations with the 1st-order to the 5th-order bedrocks
386 (AST=10 m). When the WTD is less than 1 m, data points from different bedrock settings almost
387 fall on a single curve because water table is dominated by the land surface topography, and the

388 approximately linear curve on semi-log plot (Figure 9) suggests that the saturated area follows an
389 exponential relationship with respect to mean water table depth, which is in agreement with Niu
390 et al. (2005) who obtained an exponential relationship between the fraction of saturated area and
391 water table depth by representing the CDF of topographic wetness index using an exponential
392 function. However, when the WTD is larger than 1 m, the data points from different bedrocks
393 deviate from each other because the effect of bedrock on saturated area kicks in.

394 **3.6 Unifying saturation excess runoff models**

395 The TOPMODEL and VIC-type model are popular hydrological models for modeling
396 saturation excess runoff. They are usually considered to have distinct conceptualizations on the
397 physical processes. The fundamental assumption in TOPMODEL is that the gradient of water
398 table equals the gradient of land surface; in other words, the shape of water table is dominated by
399 land surface topography (Beven & Kirkby, 1979). While, the VIC-type model considers the
400 catchment as a collection of storage elements with different storage capacities represented by a
401 probability distribution (Liang et al., 1994; Moore, 2007). What is the assumption of water table
402 configuration in VIC-type model corresponding to the distribution of water storage? To answer
403 this question, we propose to evaluate the VIC-type model from the perspective of water table
404 configuration which controls to the spatial distribution of water storage.

405 As shown in Figure 10a, the VIC-type model assumes that water storage in the unsaturated
406 area is spatially uniform. Water storage mainly consists of the groundwater below the water table
407 especially for soils with small capillary effects. Thus, the VIC-type model approximately assumes
408 that groundwater storage is spatially uniform in the unsaturated area, which means that water table
409 is parallel to bedrock surface. Therefore, the VIC-type model assumes that the shape of water
410 table is dominated by bedrock topography.

411 Both the TOPMODEL and VIC-type model assume that the water table rises or falls by
412 spatially uniform amounts, meaning that the shape of water table does not change with water table
413 depths. However, results from Section 3.2 have demonstrated that the shape of water table changes
414 significantly over a wide range of water table depths, i.e., from land surface dominated to bedrock
415 dominated. Figure 10b shows the locations of these two kinds of water tables along a
416 representative hillslope profile in nature. The colors of the double-headed arrow in Figure 10b
417 indicate the transition of water table types with water table depth. Considering their assumptions
418 on the water table configuration, TOPMODEL is more reasonable in the red zone where the water
419 table is more land surface dominated, whereas, the VIC-type model is more reasonable in the blue
420 zone where the water table is more bedrock dominated . It has been discussed in Sections 3.2 that
421 neither land surface nor bedrock surface provides a reasonable estimate of the water table
422 configuration when water table is at the middle range of locations between land surface and
423 bedrock surface indicated by the white color in the double-headed arrow; therefore, neither model
424 is suitable under this condition. While, if the topographies of bedrock and land surface are
425 identical, it can be speculated both the TOPMODEL and VIC-type model are reasonable for land
426 surface-dominated water table or bedrock-dominated water table.

427 The dynamic of water table configuration with water table depth provides a framework for
428 unifying saturation excess runoff models. When water table is dominated by land surface as
429 assumed in the TOPMODEL, the available space for water storage is same over the unsaturated
430 area, thereby water storage capacity is spatially uniform. Whilst, when water table is dominated
431 by bedrock surface, the existing water storage in the unsaturated area is spatially uniform as
432 assumed by VIC-type model. In the future investigations, it might be possible to have a new
433 method to smoothly characterize the spatial distribution of water storage (or water storage

434 capacity) from land surface-dominated water table to bedrock-dominated water table, and this new
435 method enables a unified saturation excess runoff model suitable for different water table
436 conditions with the TOPMODEL and VIC-type model as the two endmembers.

437

438 **4. Conclusion**

439 The spatial pattern of groundwater table and the corresponding distribution of water storage
440 are recognized as crucial determinants of saturation excess runoff generation at the catchment
441 scale. This paper evaluated the control of topography of land surface and that of bedrock surface
442 on the configuration of groundwater table at different water table depths. To study the role of
443 bedrock topography, a series of synthetic bedrocks owning different correlations with land surface
444 topography were generated. The steady-state water tables were obtained from numerical
445 simulations using MODFLOW (USG). Water table configuration at the catchment scale was
446 found to be determined by the vertical distance from water table to land surface and bedrock
447 surface. When water table is close to the land surface, land surface is a good proxy of water table;
448 and when the water table is close to the bedrock, bedrock is a good proxy of water table. Results
449 showed that the spatial distribution of water storage, quantified through the empirical cumulative
450 distribution function, changes with water table depth systematically, and the water storage was
451 more uniform when the water table is dominated by bedrock especially when the bedrock has less
452 microtopographic features. The capillary effects of soil were found to decrease the difference of
453 the spatial distribution of water storage between different water table depth conditions. Moreover,
454 it was found that the percentage of saturated area on the land surface follows an exponential
455 relationship with mean water table depth, and the relationship can be divided into two regimes
456 based on the impacts of bedrock topography.

457 This paper provided a framework to unify the TOPMODEL and VIC-type model based on
458 their assumptions on water table configuration. The assumed water table in TOPMODEL is
459 dominated by land surface, suggesting a uniform water storage capacity in the unsaturated area;
460 whilst the assumed water table in VIC-type model is bedrock dominated, and denotes a uniform
461 water storage in the unsaturated area. Different saturation excess runoff models are possible to be
462 unified by a single model which is capable to characterize the full spectrum of water table
463 configurations: land surface-dominated type, bedrock-dominated type, and the transition between
464 them.

465 The findings of this study contribute to a better understanding of the spatial distribution of
466 groundwater table and water storage at the catchment scale, representing a further step towards
467 developing process-based hydrological models for modeling the saturation excess runoff
468 generation. However, these findings may be somewhat limited by the modeling sets applied in
469 this study. First, it assumes homogenous geological properties and recharge in the model area;
470 secondly, it assumes a hydrostatic soil moisture profile above groundwater table rather than fully
471 coupling the saturated zone and unsaturated zone. Further studies, which consider more
472 comprehensive spatial heterogeneity of catchment properties, could be undertaken.

473

474 **Acknowledgement**

475 This research was funded in part under award CBET-1804770 from National Science
476 Foundation (NSF). Yao would like to acknowledge the financial support provided by the
477 University of Central Florida through the Trustees Doctoral Fellowship. The catchment boundary
478 can be downloaded from
479 <https://water.usgs.gov/GIS/metadata/usgswrd/XML/streamgagebasins.xml>. The Digital elevation

480 models (DEMs) at around 30 m resolution is available from National Map website
481 (<https://viewer.nationalmap.gov/basic/>). The bedrock topography map of the Ozark, Illinois,
482 Indiana, and Kentucky (OIINK) Region is available from
483 [https://clearinghouse.isgs.illinois.edu/data/geology/geologic-and-geophysical-maps-ozark-](https://clearinghouse.isgs.illinois.edu/data/geology/geologic-and-geophysical-maps-ozark-illinois-indiana-and-kentucky-oiink-region)
484 [illinois-indiana-and-kentucky-oiink-region](https://clearinghouse.isgs.illinois.edu/data/geology/geologic-and-geophysical-maps-ozark-illinois-indiana-and-kentucky-oiink-region).

485

486 **References**

- 487 Appels, W. M., Bogaart, P. W., & van der Zee, S. E. A. T. M. (2017). Feedbacks Between Shallow
488 Groundwater Dynamics and Surface Topography on Runoff Generation in Flat Fields.
489 *Water Resources Research*, 53(12), 10336–10353. <https://doi.org/10.1002/2017WR020727>
- 490 Bachmair, S., & Weiler, M. (2012). Hillslope characteristics as controls of subsurface flow
491 variability. *Hydrology and Earth System Sciences*, 16(10), 3699–3715.
492 <https://doi.org/10.5194/hess-16-3699-2012>
- 493 Berghuijs, W. R., Hartmann, A., & Woods, R. A. (2016). Streamflow sensitivity to water storage
494 changes across Europe: Streamflow Sensitivity to Storage Change. *Geophysical Research*
495 *Letters*, 43(5), 1980–1987. <https://doi.org/10.1002/2016GL067927>
- 496 Beven, K. J., & Kirkby, M. J. (1979). A physically based, variable contributing area model of basin
497 hydrology. *Hydrological Sciences Journal*, 24(1), 43–69.
498 <https://doi.org/10.1080/02626667909491834>
- 499 Brooks, R. H., & Corey, A. T. (1964). *Hydraulic properties of porous media* (Vol. no. 3). Colorado
500 State University, Fort Collins, CO.
- 501 Cardenas, M. B. (2007). Potential contribution of topography-driven regional groundwater flow to
502 fractal stream chemistry: Residence time distribution analysis of Tóth flow. *Geophysical*

503 *Research Letters*, 34(5). <https://doi.org/10.1029/2006GL029126>

504 Condon, L. E., & Maxwell, R. M. (2015). Evaluating the relationship between topography and
505 groundwater using outputs from a continental-scale integrated hydrology model. *Water*
506 *Resources Research*, 51(8), 6602–6621. <https://doi.org/10.1002/2014WR016774>

507 Condon, L. E., Atchley, A. L., & Maxwell, R. M. (2020). Evapotranspiration depletes groundwater
508 under warming over the contiguous United States. *Nature Communications*, 11(1), 873.
509 <https://doi.org/10.1038/s41467-020-14688-0>

510 Condon, L. E., Markovich, K. H., Kelleher, C. A., McDonnell, J. J., Ferguson, G., & McIntosh, J.
511 C. (2020). Where Is the Bottom of a Watershed? *Water Resources Research*, 56(3),
512 e2019WR026010. <https://doi.org/10.1029/2019WR026010>

513 Cuthbert, M. O., Gleeson, T., Moosdorf, N., Befus, K. M., Schneider, A., Hartmann, J., & Lehner,
514 B. (2019). Global patterns and dynamics of climate–groundwater interactions. *Nature*
515 *Climate Change*, 9(2), 137–141. <https://doi.org/10.1038/s41558-018-0386-4>

516 Desbarats, A. J., Logan, C. E., Hinton, M. J., & Sharpe, D. R. (2002). On the kriging of water table
517 elevations using collateral information from a digital elevation model. *Journal of*
518 *Hydrology*, 255(1–4), 25–38.

519 Detty, J. M., & McGuire, K. J. (2010). Topographic controls on shallow groundwater dynamics:
520 implications of hydrologic connectivity between hillslopes and riparian zones in a till
521 mantled catchment. *Hydrological Processes*, 24(16), 2222–2236.
522 <https://doi.org/10.1002/hyp.7656>

523 Devito, K., Creed, I., Gan, T., Mendoza, C., Petrone, R., Silins, U., & Smerdon, B. (2005). A
524 framework for broad-scale classification of hydrologic response units on the Boreal Plain:
525 is topography the last thing to consider? *Hydrological Processes*, 19(8), 1705–1714.

526 <https://doi.org/10.1002/hyp.5881>

527 Dhakal, A. S., & Sullivan, K. (2014). Shallow groundwater response to rainfall on a forested
528 headwater catchment in northern coastal California: implications of topography, rainfall,
529 and throughfall intensities on peak pressure head generation. *Hydrological Processes*,
530 28(3), 446–463. <https://doi.org/10.1002/hyp.9542>

531 Fan, Y., & Bras, R. L. (1998). Analytical solutions to hillslope subsurface storm flow and saturation
532 overland flow. *Water Resources Research*, 34(4), 921–927.
533 <https://doi.org/10.1029/97WR03516>

534 Ferguson, I. M., & Maxwell, R. M. (2010). Role of groundwater in watershed response and land
535 surface feedbacks under climate change. *Water Resources Research*, 46, W00F02.
536 <https://doi.org/10.1029/2009WR008616>

537 Freer, J., McDonnell, J., Beven, K. J., Brammer, D., Burns, D., Hooper, R. P., & Kendal, C. (1997).
538 Topographic controls on subsurface storm flow at the hillslope scale for two hydrologically
539 distinct small catchments. *Hydrological Processes*, 11(9), 1347–1352.

540 Freer, J., McDonnell, J. J., Beven, K. J., Peters, N. E., Burns, D. A., Hooper, R. P., et al. (2002).
541 The role of bedrock topography on subsurface storm flow. *Water Resources Research*,
542 38(12), 1269. <https://doi.org/10.1029/2001WR000872>

543 Freeze, R. A., & Cherry, J. A. (1979). *Groundwater*. Englewood Cliffs, NJ: Prentice Hall.

544 Gao, Y., Yao, L., Chang, N.-B., & Wang, D. (2020). Diagnosis toward predicting mean annual
545 runoff in ungauged basins. *Hydrology and Earth System Sciences Discussion* (preprint).
546 <https://doi.org/10.5194/hess-2020-353>, in review.

547 Gleeson, T., & Manning, A. H. (2008). Regional groundwater flow in mountainous terrain: Three-
548 dimensional simulations of topographic and hydrogeologic controls. *Water Resources*

549 *Research*, 44, W10403. <https://doi.org/10.1029/2008WR006848>

550 Goderniaux, P., Davy, P., Bresciani, E., de Dreuzy, J.-R., & Borgne, T. L. (2013). Partitioning a
551 regional groundwater flow system into shallow local and deep regional flow compartments.
552 *Water Resources Research*, 49, 2274–2286. <https://doi.org/10.1002/wrcr.20186>

553 Grayson, R., & Western, A. (2001). Terrain and the distribution of soil moisture. *Hydrological*
554 *Processes*, 15(13), 2689–2690. <https://doi.org/10.1002/hyp.479>

555 Haitjema, H. M., & Mitchell-Bruker, S. (2005). Are Water Tables a Subdued Replica of the
556 Topography? *Ground Water*, 43(6), 781–786.

557 Hooshyar, M., & Wang, D. (2016). An analytical solution of Richards' equation providing the
558 physical basis of SCS curve number method and its proportionality relationship. *Water*
559 *Resources Research*, 52(8), 6611–6620. <https://doi.org/10.1002/2016WR018885>

560 Hutchinson, D. G., & Moore, R. D. (2000). Throughflow variability on a forested hillslope
561 underlain by compacted glacial till. *Hydrological Processes*, 14, 1751–1766.

562 Jiang, X.-W., Wan, L., Cardenas, M. B., Ge, S., & Wang, X.-S. (2010). Simultaneous rejuvenation
563 and aging of groundwater in basins due to depth-decaying hydraulic conductivity and
564 porosity. *Geophysical Research Letters*, 37(5), L05403.
565 <https://doi.org/10.1029/2010GL042387>

566 Kollet, S. J., & Maxwell, R. M. (2008). Capturing the influence of groundwater dynamics on land
567 surface processes using an integrated, distributed watershed model. *Water Resources*
568 *Research*, 44, W02402. <https://doi.org/10.1029/2007WR006004>

569

570 Liang, X., Lettenmaier, D. P., Wood, E. F., & Burges, S. J. (1994). A simple hydrologically based
571 model of land surface water and energy fluxes for general circulation models. *Journal of*

572 *Geophysical Research: Atmospheres*, 99(D7), 14415–14428.

573 Liang, X., Xie, Z., & Huang, M. (2003). A new parameterization for surface and groundwater
574 interactions and its impact on water budgets with the variable infiltration capacity (VIC)
575 land surface model. *Journal of Geophysical Research*, 108(D16), 8613.
576 <https://doi.org/10.1029/2002JD003090>

577 Maxwell, R. M., & Condon, L. E. (2016). Connections between groundwater flow and
578 transpiration partitioning. *Science*, 353(6297), 377–380.
579 <https://doi.org/10.1126/science.aaf7891>

580 McDonnell, J. J., Freer, J., Hooper, R., Kendall, C., Burns, D., Beven, K., & Peters, J. (1996). New
581 method developed for studying flow on hillslopes. *Eos, Transactions American*
582 *Geophysical Union*, 77(47), 465–472. <https://doi.org/10.1029/96EO00306>

583 van Meerveld, H. J., Seibert, J., & Peters, N. E. (2015). Hillslope-riparian-stream connectivity and
584 flow directions at the Panola Mountain Research Watershed. *Hydrological Processes*,
585 29(16), 3556–3574. <https://doi.org/10.1002/hyp.10508>

586 Micallef, A., Person, M., Haroon, A., Weymer, B. A., Jegen, M., Schwalenberg, K., et al. (2020).
587 3D characterisation and quantification of an offshore freshened groundwater system in the
588 Canterbury Bight. *Nature Communications*, 11(1), 1372. [https://doi.org/10.1038/s41467-](https://doi.org/10.1038/s41467-020-14770-7)
589 [020-14770-7](https://doi.org/10.1038/s41467-020-14770-7)

590 Michael G. McDonald & Arlen W. Harbaugh. (1998). *A modular three-dimensional finite-*
591 *difference ground-water flow model*. US Geological Survey.

592 Montgomery, D. R., & Foufoula-Georgiou, E. (1993). Channel network source representation
593 using digital elevation models. *Water Resources Research*, 29(12), 3925–3934.
594 <https://doi.org/10.1029/93WR02463>

595 Moore, R. J. (1985). The probability-distributed principle and runoff production at point and basin
596 scales. *Hydrological Sciences Journal*, 30(2), 273–297.
597 <https://doi.org/10.1080/02626668509490989>

598 Moore, R. J. (2007). The PDM rainfall-runoff model. *Hydrology and Earth System Sciences*, 11(1),
599 483–499. <https://doi.org/10.5194/hess-11-483-2007>

600 Niu, G.-Y., Yang, Z.-L., Dickinson, R. E., & Gulden, L. E. (2005). A simple TOPMODEL-based
601 runoff parameterization (SIMTOP) for use in global climate models. *Journal of*
602 *Geophysical Research*, 110, D21106. <https://doi.org/10.1029/2005JD006111>

603 Panday, S., Langevin, C. D., Niswonger, R. G., Ibaraki, M., & Hughes, J. D. (2013). *MODFLOW–*
604 *USG version 1: An unstructured grid version of MODFLOW for simulating groundwater*
605 *flow and tightly coupled processes using a control volume finite-difference formulation*
606 (book 6 A45). U.S. Geological Survey Techniques and Methods. Retrieved from
607 <https://pubs.usgs.gov/tm/06/a45>.

608 Penna, D., Mantese, N., Hopp, L., Fontana, G. D., & Borga, M. (2015). Spatio-temporal variability
609 of piezometric response on two steep alpine hillslopes. *Hydrological Processes*, 29, 198–
610 211. <https://doi.org/10.1002/hyp.10140>

611 Rawls, W. J., Brakensiek, D. L., & Saxton, K. E. (1982). Estimating soil water properties.
612 *Transactions of the ASAE*, 25(5), 1316–1320. <https://doi.org/10.13031/2013.33720>

613 Rempe, D. M., & Dietrich, W. E. (2014). A bottom-up control on fresh-bedrock topography under
614 landscapes. *Proceedings of the National Academy of Sciences*, 111(18), 6576–6581.

615 Rinderer, M., van Meerveld, H. J., & Seibert, J. (2014). Topographic controls on shallow
616 groundwater levels in a steep, prealpine catchment: When are the TWI assumptions valid?
617 *Water Resources Research*, 50(7), 6067–6080. <https://doi.org/10.1002/2013WR015009>

618 Shaman, J., Stieglitz, M., Engel, V., Koster, R., & Stark, C. (2002). Representation of subsurface
619 storm flow and a more responsive water table in a TOPMODEL-based hydrology model.
620 *Water Resources Research*, 38(8), 31-1-31–16. <https://doi.org/10.1029/2001WR000636>

621 Sivapalan, M., Beven, K., & Wood, E. F. (1987). On hydrologic similarity: 2. A scaled model of
622 storm runoff production. *Water Resources Research*, 23(12), 2266–2278.
623 <https://doi.org/10.1029/WR023i012p02266>

624 Sivapalan, M., Woods, R. A., & Kalma, J. D. (1997). Variable bucket representation of
625 TOPMODEL and investigation of the effects of rainfall heterogeneity. *Hydrological*
626 *Processes*, 11, 24.

627 Soyly, M. E., Istanbuluoglu, E., Lenters, J. D., & Wang, T. (2011). Quantifying the impact of
628 groundwater depth on evapotranspiration in a semi-arid grassland region. *Hydrology and*
629 *Earth System Sciences*, 15(3), 787–806. <https://doi.org/10.5194/hess-15-787-2011>

630 Spence, C., Guan, X. J., Phillips, R., Hedstrom, N., Granger, R., & Reid, B. (2009). Storage
631 dynamics and streamflow in a catchment with a variable contributing area. *Hydrological*
632 *Processes*, 24(16), 2209–2221. <https://doi.org/10.1002/hyp.7492>

633 St. Clair, J., Moon, S., Holbrook, W. S., Perron, J. T., Riebe, C. S., Martel, S. J., et al. (2015).
634 Geophysical imaging reveals topographic stress control of bedrock weathering. *Science*,
635 350(6260), 534–538. <https://doi.org/10.1126/science.aab2210>

636 Toth, J. (1963). A theoretical analysis of groundwater flow in small drainage basins. *Journal of*
637 *Geophysical Research*, 68(16), 4795–4812. <https://doi.org/10.1029/JZ068i016p04795>

638 Troch, P., Mancini, M., Paniconi, C., & Wood, E. F. (1993). Evaluation of a distributed catchment
639 scale water balance model. *Water Resources Research*, 29(6), 1805–1817.
640 <https://doi.org/10.1029/93WR00398>

641 Troch, P., van Loon, E., & Hilberts, A. (2002). Analytical solutions to a hillslope-storage kinematic
642 wave equation for subsurface flow. *Advances in Water Resources*, 25(6), 637–649.
643 [https://doi.org/10.1016/S0309-1708\(02\)00017-9](https://doi.org/10.1016/S0309-1708(02)00017-9)

644 Tromp-van Meerveld, H. J., & McDonnell, J. J. (2006). Threshold relations in subsurface
645 stormflow: 1. A 147-storm analysis of the Panola hillslope. *Water Resources Research*,
646 42(2), W02410. <https://doi.org/10.1029/2004WR003778>

647 Yao, L., Wang, D., Hooshyar, M., Singh, A., & Sivapalan, M. (2018). Time Compression
648 Approximation Relationship for Infiltration in the Presence of a Shallow Water Table:
649 Evaluating the Role of Péclet Number. *Water Resources Research*, 54(11), 9384–9397.
650 <https://doi.org/10.1029/2018WR023293>

651 Yao, L., Libera, D. A., Kheimi, M., Sankarasubramanian, A., & Wang, D. (2020). The Roles of
652 Climate Forcing and Its Variability on Streamflow at Daily, Monthly, Annual, and Long-
653 Term Scales. *Water Resources Research*, 56(7), e2020WR027111.
654 <https://doi.org/10.1029/2020WR027111>

655 Zhang, X., Jiao, J. J., Li, H., Luo, X., & Kuang, X. (2020). Effects of Downward Intrusion of
656 Saline Water on Nested Groundwater Flow Systems. *Water Resources Research*, 56(10),
657 e2020WR028377. <https://doi.org/10.1029/2020WR028377>

658 Zhao, R.-J. (1992). The Xinanjiang model applied in China. *Journal of Hydrology*, 135(1–4), 371–
659 381. [https://doi.org/10.1016/0022-1694\(92\)90096-E](https://doi.org/10.1016/0022-1694(92)90096-E)

660 Zimmer, M. A., & McGlynn, B. L. (2017). Ephemeral and intermittent runoff generation processes
661 in a low relief, highly weathered catchment. *Water Resources Research*, 53(8), 7055–7077.
662 <https://doi.org/10.1002/2016WR019742>

663 **Figure captions:**

664 Figure 1: The Crab Orchard Creek catchment in Illinois (USGS gauge ID: 05597500): (a) the land
665 surface topography and channel network with 30 m resolution; and (b) the observed bedrock
666 topography with 100 m resolution.

667

668 Figure 2: The topography of the generated bedrock based on different orders of stream network.
669 The values in the figure represent the relative elevation (m) above the lowest point of the generated
670 bedrock.

671

672 Figure 3: The empirical cumulative distribution function (CDF) of the normalized maximum
673 storage capacity (a) in models with different shapes of bedrock but with the same average soil
674 thickness (= 10 m); and (b) in models with the 2nd-order bedrock but with different average soil
675 thickness (AST).

676

677 Figure 4: The simulated water table elevations for the 5 synthetic bedrocks with 10 m of average
678 soil thickness when the mean water table depth (WTD) equals 1.5 m (a1-e1), 4 m (a2-e2), and 8
679 m (a3-e3).

680

681 Figure 5: The water tables for the 2nd-order bedrock with 13 m of average soil thickness when (a)
682 the mean water table depth is 8 m (i.e., the mean vertical distance between water table and bedrock
683 surface is 5 m); (b) the mean water table depth is 11 m (i.e., the mean vertical distance between

684 water table and bedrock surface is 2 m).

685

686 Figure 6: The standard deviation of the vertical distance between water table and land surface or
687 bedrock surface versus the mean water table depth when the average soil thickness is 10 m.

688

689 Figure 7: The spatial distributions of water storage for sand under different mean water table depths
690 (WTD) when the average soil thickness is 10 m, and the black curve represents the maximum
691 storage capacity.

692

693 Figure 8: The spatial distributions of water storage for clay under different mean water table depths
694 (WTD) when the average soil thickness is 10 m, and the black curve represents the maximum
695 storage capacity.

696

697 Figure 9: The relationship between saturated area percentage and mean water table depth (WTD)
698 when the average soil thickness is 10 m. When $WTD < 1$ m (denoted by the black dashed line),
699 saturated area percentage is dominated by land surface.

700

701 Figure 10: (a) The conceptualization of water storage in the VIC-type model: $F(C)$ is the fraction
702 of the catchment area for which the storage capacity is less than or equal to C ; S_0 is the initial soil
703 water storage; P is the precipitation which is partitioned into the soil wetting (W) and runoff (R).

704 (b) The configuration of groundwater table at different water table depths along a representative

705 hillslope profile in nature. The colors in the double-headed arrow indicate the transition of water

706 table control.

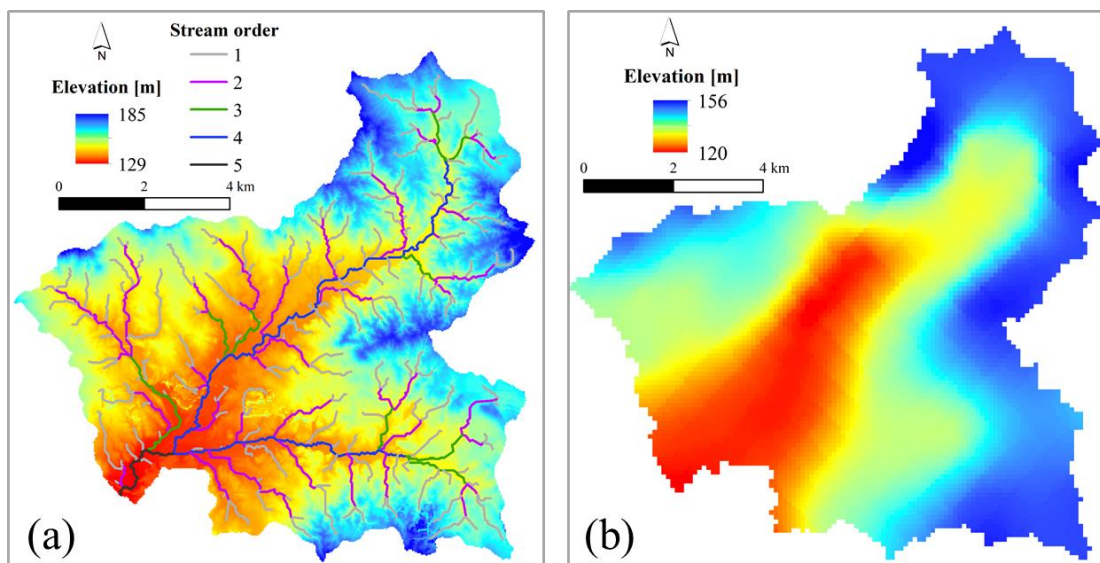
707

708 Table 1 Hydraulic parameters of the Brooks-Corey model for sand and clay (Rawls et al., 1982)

Soil type	θ_s [-]	θ_r [-]	$ \varphi_a $ [m]	λ [-]
Sand	0.417	0.020	0.072	0.592
Clay	0.385	0.090	0.373	0.131

709

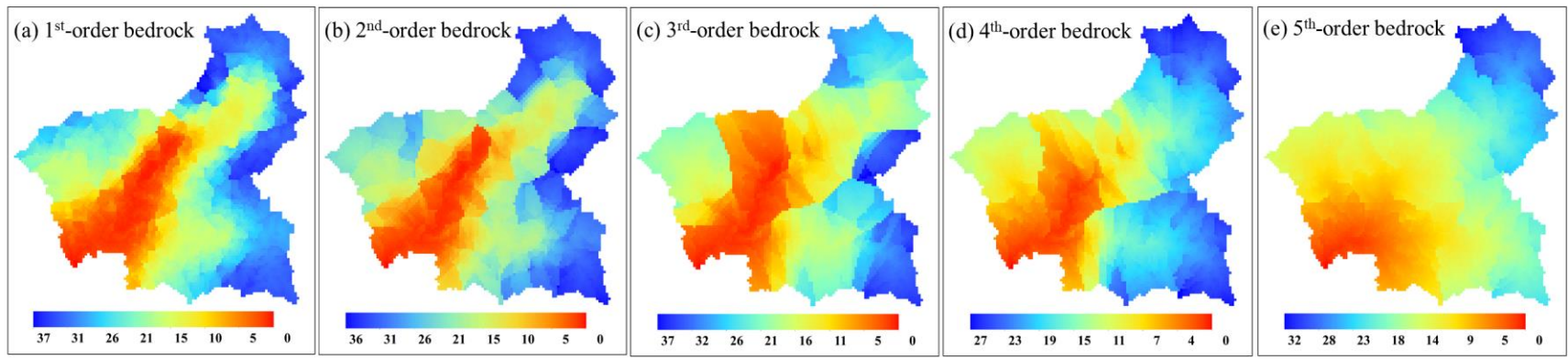
710



711

712 Figure 1: The Crab Orchard Creek catchment in Illinois (USGS gauge ID: 05597500): (a) the
713 land surface topography and channel network with 30 m resolution; and (b) the observed bedrock
714 topography with 100 m resolution.

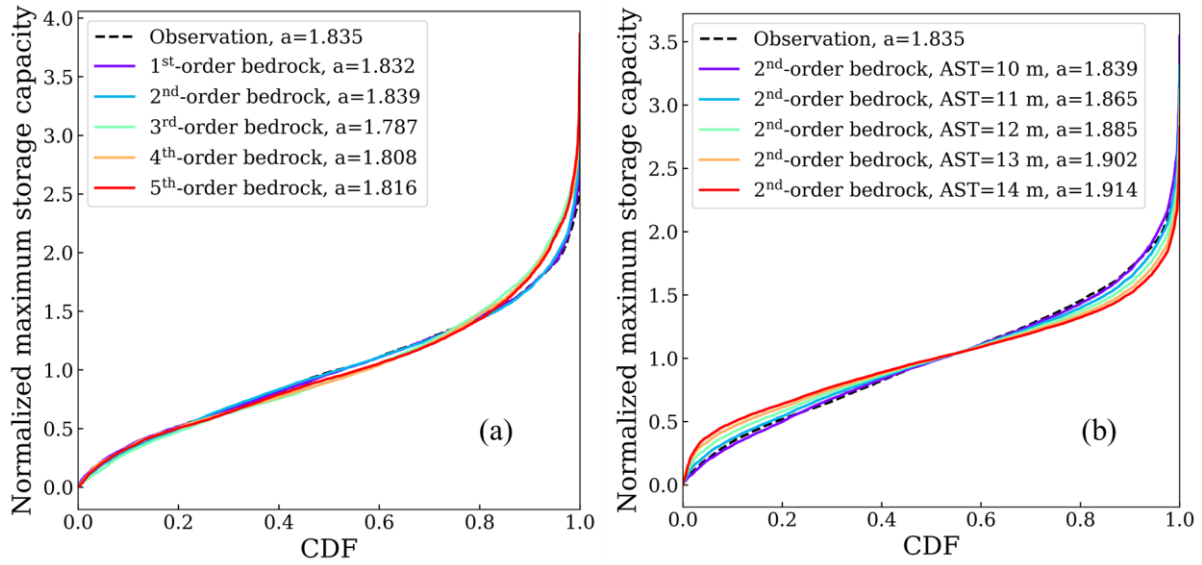
715



716

717 Figure 2: The topography of the generated bedrock based on different orders of stream network. The values in the figure represent the
 718 relative elevation (m) above the lowest point of the generated bedrock.

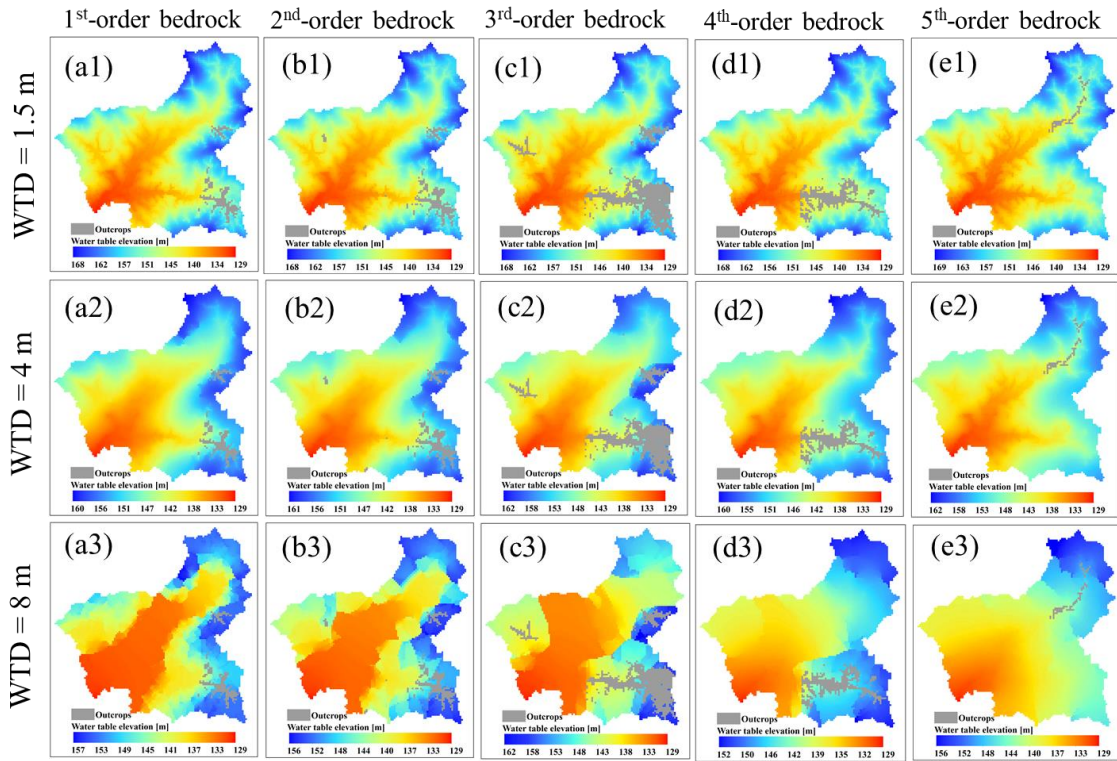
719



720

721 Figure 3: The empirical cumulative distribution function (CDF) of the normalized maximum
 722 storage capacity (a) in models with different shapes of bedrock but with the same average soil
 723 thickness (= 10 m); and (b) in models with the 2nd-order bedrock but with different average soil
 724 thickness (AST).

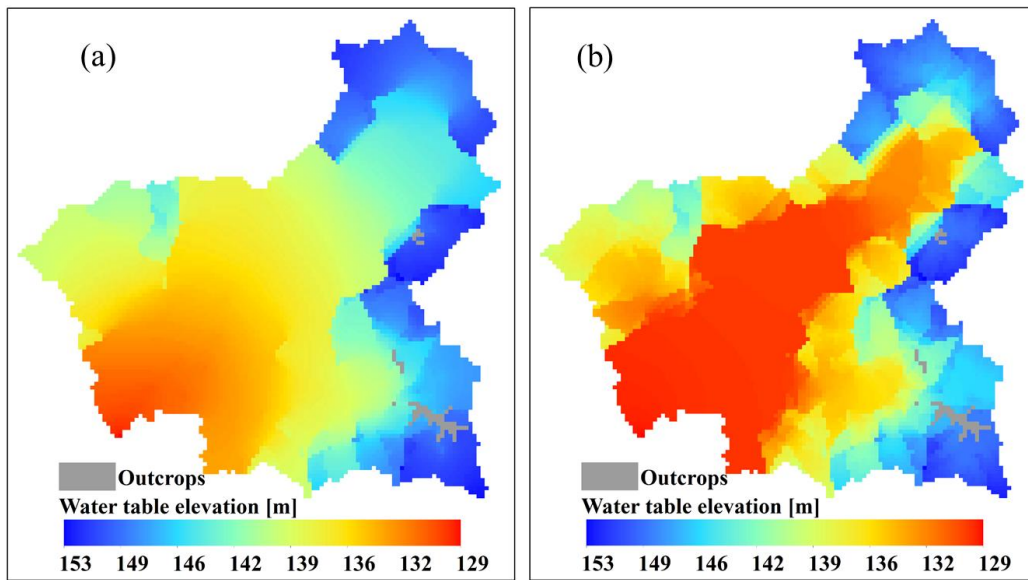
725



726

727 Figure 4: The simulated water table elevations for the 5 synthetic bedrocks with 10 m of average
728 soil thickness when the mean water table depth (WTD) equals 1.5 m (a1-e1), 4 m (a2-e2), and 8
729 m (a3-e3).

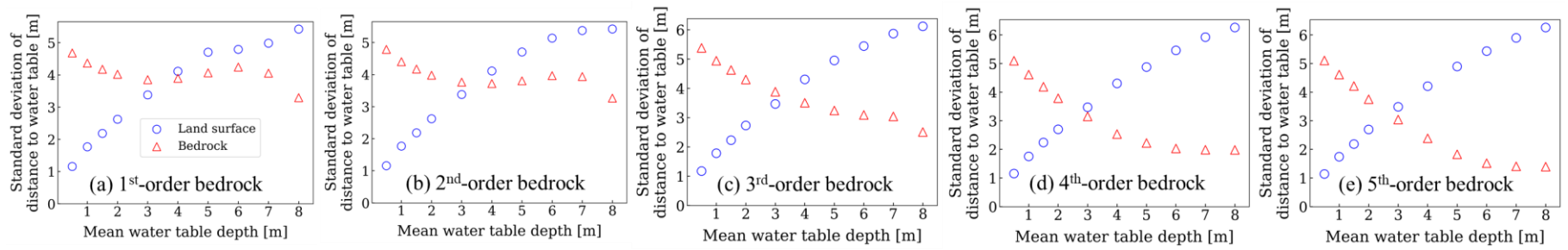
730



731

732 Figure 5: The water tables for the 2nd-order bedrock with 13 m of average soil thickness when (a)
733 the mean water table depth is 8 m (i.e., the mean vertical distance between water table and
734 bedrock surface is 5 m); (b) the mean water table depth is 11 m (i.e., the mean vertical distance
735 between water table and bedrock surface is 2 m).

736

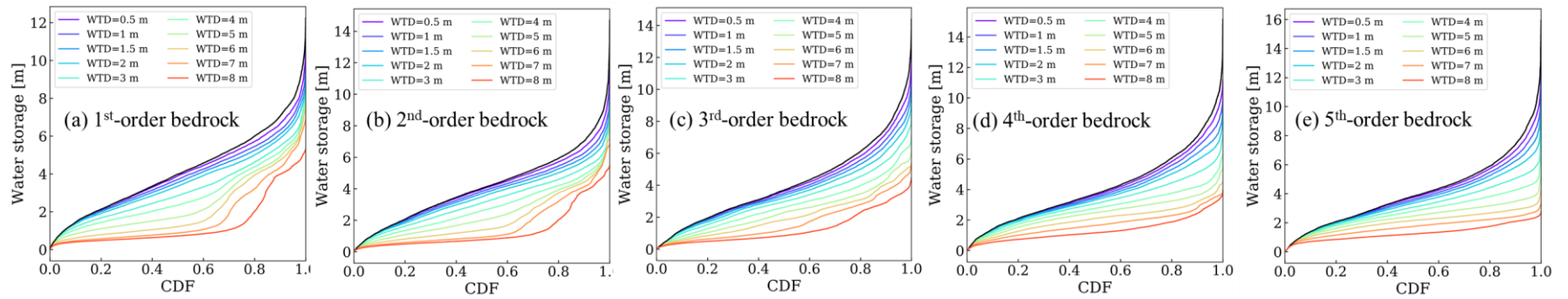


737

738 Figure 6: The standard deviation of the vertical distance between water table and land surface or bedrock surface versus the mean
739 water table depth when the average soil thickness is 10 m.

740

741

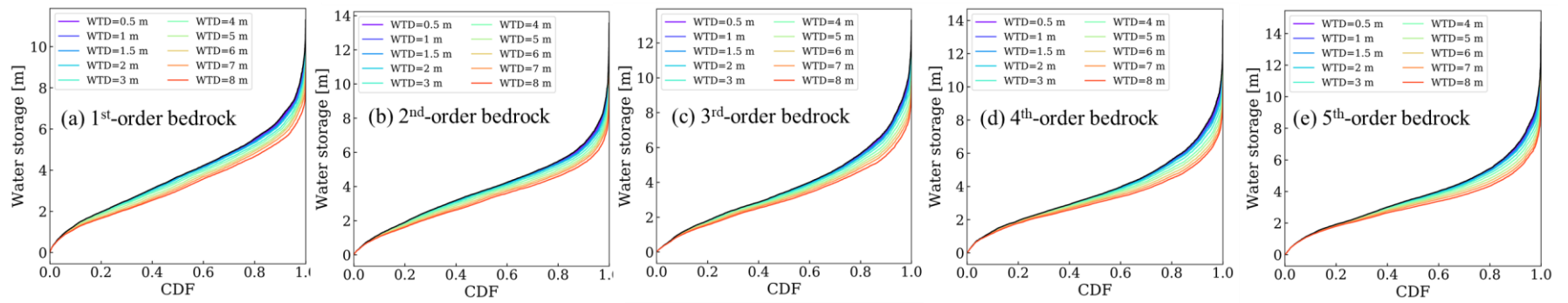


742

743

744

Figure 7: The spatial distributions of water storage for sand under different mean water table depths (WTD) when the average soil thickness is 10 m, and the black curve represents the maximum storage capacity.

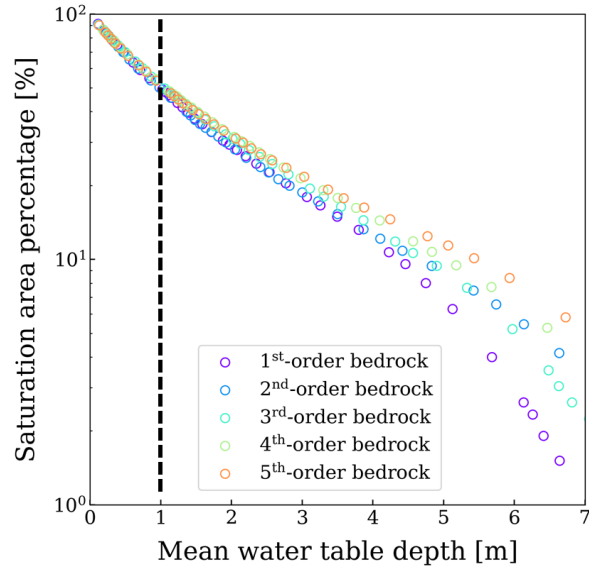


745

746

747

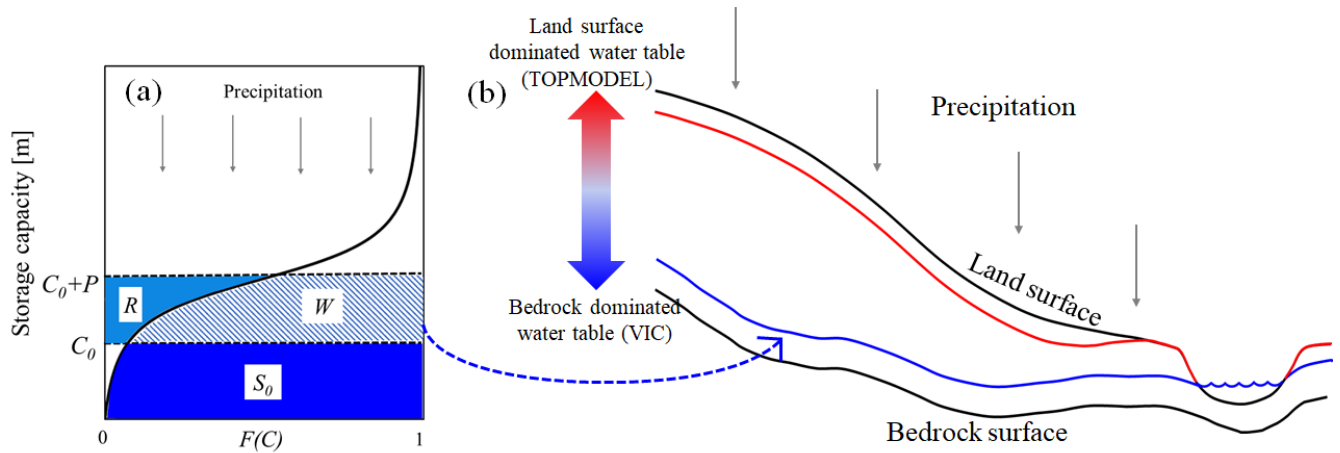
Figure 8: The spatial distributions of water storage for clay under different mean water table depths (WTD) when the average soil thickness is 10 m, and the black curve represents the maximum storage capacity.



748

749 Figure 9: The relationship between saturated area percentage and mean water table depth (WTD)
 750 when the average soil thickness is 10 m. When WTD < 1 m (denoted by the black dashed line),
 751 saturated area percentage is dominated by land surface.

752



753

754 Figure 10: (a) The conceptualization of water storage in the VIC-type model: $F(C)$ is the
755 fraction of the catchment area for which the storage capacity is less than or equal to C ; S_0 is the
756 initial soil water storage; P is the precipitation which is partitioned into the soil wetting (W) and
757 runoff (R). (b) The configuration of groundwater table at different water table depths along a
758 representative hillslope profile in nature. The colors in the double-headed arrow indicate the
759 transition of water table control.